

# A TOY MODEL FOR THE ELECTROMAGNETIC OUTPUT OF NEUTRON-STAR MERGER PROMPT COLLAPSE TO A BLACK HOLE: MAGNETIZED NEUTRON-STAR COLLISIONS

ANTONIOS NATHANAIL

Institut für Theoretische Physik, Max-von-Laue-Strasse 1, D-60438 Frankfurt, Germany

## ABSTRACT

We present a systematic study of magnetised neutron star head on collisions. We investigate the resulting magnetic field geometries as the two neutron stars merge. Furthermore, we analyze the luminosity produced in these collisions and monitor the evolution of the magnetic fields from the time of merger until the subsequent production of a black hole. At the time of black hole formation the luminosity peaks and rings-down following the decay of the electromagnetic fields. A comparison is presented for three different cases, one where the initial magnetic field in both neutron stars is aligned, one where they are anti-aligned and also one case where they initially have unequal magnetic field strength. We identify regions and set limits so that pair creation and magnetic reconnection would occur in this scenario, and further discuss limits and differences in the radiated energy. This study should be regarded as a toy model of the case where the remnant, of a binary neutron star merger, undergoes a prompt collapse to a black hole with a negligible surrounding disk. We note that the generated electromagnetic pulses resembles the fast radio bursts phenomenology. We consider implications on the high mass mergers leading to a fast prompt collapse to a black hole and the expected flux to be observed at a distance similar to the binary neutron star gravitational wave detection GW190425.

*Keywords:* Neutron stars, Compact objects, Gravitational waves, Magnetohydrodynamical simulations

## 1. INTRODUCTION

The coincident detection of gravitational waves (GW) from binary neutron star mergers and the detection of a short gamma-ray burst (sGRB) together with the subsequent detection of afterglows across the electromagnetic (EM) spectrum has opened up a new era in Astronomy and firmly established the connection of binary neutron star mergers with sGRB (Abbott et al. 2017). This new observation has given a lot of insight in such a process and initiated a deeper theoretical study and extensive numerical modeling of such systems which can have a very rich phenomenology due to the different binary properties, as the massive case of GW190425 (The LIGO Scientific Collaboration et al. 2020), which had a total mass of  $3.4^{+0.3}_{-0.1} M_{\odot}$ , and there is a claim of an EM follow up detection (Pozenenko et al. 2019).

The important role of neutrinos in these explosions and the subsequent r-processing element production which will still have unique signaling is flourishing these last years (Sekiguchi et al. 2015, 2016; Palenzuela et al. 2015; Hotokezaka & Piran 2015; Hotokezaka et al. 2017; Dietrich & Ujevic 2017; Radice et al. 2016; Lehner et al. 2016; Sekiguchi et al. 2016; Foucart et al. 2016; Bovard et al. 2017; Dietrich et al. 2017a,b; Radice et al. 2018;

Papenfort et al. 2018; Fernández et al. 2018; Siegel & Metzger 2018). The amount of physics one can extract from these events is enormous. The possibility of a long lived remnant, its properties (see e.g. (Hanauske et al. 2017; Kastaun et al. 2016b; Fujibayashi et al. 2017; Ciolfi et al. 2017; Fujibayashi et al. 2018)) and its consequences to electromagnetic modeling are essential.

The main possible outcomes of a binary neutron star merger are three: (i) a prompt collapse to a black hole (BH), (ii) a neutron star that later collapses to a BH and (iii) a stable neutron star. The (ii) scenario can be further subdivided into classes depending how long the remnant has lived. In this study we stick to the first scenario and will not go to more detail for the other cases (Baiotti & Rezzolla (2017); Nathanail et al. (2019) for reviews). When the threshold mass is above a certain limit then this is the outcome of the merger remnant, the prompt collapse to a BH (Bauswein et al. 2013; Köppel et al. 2019). The prompt collapse is very sensitive to the equation of state (EOS) (Hotokezaka et al. 2011).

The case of the prompt collapse to a BH has been suggested not to be so exciting electromagnetically, firstly due to the limited amount of ejected mass, but also due to the small (sometimes negligible) accretion disk left around the BH (Shibata & Taniguchi 2006; Baiotti et al. 2008; Liu et al. 2008; Hotokezaka et al. 2011; Bauswein

| model                            | $B_{1, \max}$  | $B_{1, \text{pole}}$ | $B_{2, \max}$  | $A_{b, 1}$    | $A_{b, 2}$    | $E_{\text{EM}}$       |
|----------------------------------|----------------|----------------------|----------------|---------------|---------------|-----------------------|
|                                  | [ $10^{14}$ G] | [ $10^{14}$ G]       | [ $10^{14}$ G] | [ $10^{-5}$ ] | [ $10^{-5}$ ] | [ $10^{42}$ erg]      |
| Al <sub>1</sub>                  | 1.049          | 0.15                 | 1.049          | 2.2           | 2.2           | 7.91                  |
| Al <sub>2</sub>                  | 0.104          | 0.015                | 0.104          | 0.22          | 0.22          | $7.9 \times 10^{-2}$  |
| Al <sub>3</sub>                  | 0.010          | 0.0015               | 0.010          | 0.02          | 0.02          | $7.91 \times 10^{-4}$ |
| Al <sub>4</sub>                  | 10.49          | 1.5                  | 10.49          | 22            | 22            | 791                   |
| Anti-al <sub>1</sub>             | 1.049          | 0.15                 | 1.049          | 2.2           | -2.2          | 48.18                 |
| Anti-al <sub>1</sub> , high-res. | 1.049          | 0.15                 | 1.049          | 2.2           | -2.2          | 48.18                 |
| Anti-al <sub>2</sub>             | 0.1049         | 0.015                | 0.1049         | 0.22          | -0.22         | 4.818                 |
| unequal-B                        | 1.049          | 0.15                 | 0.01           | 2.2           | 0.022         | 14.06                 |

**Table 1:** Initial parameters for the different models with aligned, anti-aligned and unequal magnetic field.  $B_{1, \max}$  is the maximum value of the magnetic field strength inside the neutron star placed 55 km at the positive part of the x- axis and  $B_{2, \max}$  the maximum of the second star placed at the same distance in the negative part respectively. Also, note that the value of the magnetic field strength at the pole  $B_{\text{pole}}$ , is an order of magnitude smaller than the maximum one for all models. Changing the sign of the vector potential gives rise to an anti-aligned dipole.

et al. 2013). Furthermore, it is not certain yet if it can actually provide an engine for a short GRB (Margalit & Metzger 2019). In order to model GRB central engines the inclusion of magnetic field is compulsory. Magnetic field amplification, a magnetized funnel and a subsequent outflow are the ingredients shown to be important in the case that the remnant of a neutron star merger collapses to a BH with some delay (Rezzolla et al. 2011; Kiuchi et al. 2014; Ruiz et al. 2016).

However, for the scenario of the prompt collapse the studies that include magnetic field are limited. Also, magnetic field amplification may be suppressed in this scenario due to the quick production of a black hole (Kiuchi et al. 2015). The torus formed around the BH may have a lifetime as small as  $t_T \sim 5 \left( \frac{M_T}{0.001 M_\odot} \right) \left( \frac{\dot{M}}{0.2 \dot{M}_\odot s^{-1}} \right)^{-1}$  ms (Ruiz & Shapiro 2017). In this amount of time no magnetized outflow is possible to be produced (Ruiz & Shapiro 2017). However, in such a short timescale the magnetic energy stored around the neutron stars will be released in a similar way of a neutron star collapse (Falcke & Rezzolla 2014; Most et al. 2018). In an ideal MHD framework this can not be captured since matter is coupled to the field. The framework we use, of general-relativistic resistive magnetohydrodynamics (GRMHD), allows for electromagnetic field evolution in vacuum. As such the magnetic field can escape once the two stars merge and leave a negligible amount of mass around them.

Studying the interactions of the magnetospheres of the two neutron stars prior to merger can set the limit to electromagnetic signals before merger. These interactions have been studied in the case of a force-free realistic magnetosphere modeling (Palenzuela 2013; Palenzuela et al. 2013b; Ponce et al. 2014). In our study we limit our focus to the merge and the subsequent evolution, since we cannot acquire reliable results prior to merger.

We begin by considering a simple head-on collision of

two magnetized neutron stars. Electromagnetically, such a scenario could have a similar signal with a prompt collapse, the case where a neutron star merger produces a remnant that quickly undergoes a gravitational collapse to a BH, and happens when the total mass is above a threshold (Hotokezaka et al. 2011; Bauswein et al. 2013; Köppel et al. 2019). One of the main features affecting the pattern and EM counterpart of BNS mergers, is the structure of the magnetic field. The simplistic approach we adopt here certainly misses the interesting aspects that would result from the dynamics of the binary affecting the EM field. However, we can provide a rough and conservative estimate of the amount of the magnetic energy, which is stored in the two magnetospheres, and will dissipate away after merger due to the lack of a significant disk to hold it. This indeed, needs to be proven from a numerical simulation perspective, since similar studies of BNS mergers undergoing prompt collapse to a BH cannot measure any EM luminosity, due to the adopted ideal MHD numerical scheme (Ruiz et al. 2018), and thus suggest that prompt collapses do not result in any EM luminosity. The resistive MHD framework that we adopt for this study, allows the evolution of the EM field in vacuum and this can yield a rough estimate of the luminosity of such an event.

The initial configuration that we use has a zero electric field in the atmosphere and is free of charges, thus suitable for an electrovacuum approach. Head on collision of self gravitating stars have been studied in order to study the conditions of BH formation (Rezzolla & Takami 2013; East & Pretorius 2013; Kellerman et al. 2010). We choose to be in the parameter space that the head on collision of two neutron stars would always form a BH. In our case the essential part is the inclusion of magnetic fields inside and outside the stars.

We explore a magnetised neutron star head on collision as a toy model to understand the electromagnetic signal

after a prompt collapse, where a negligible disk is left around the BH and as a result the magnetic field can escape in a millisecond timescale. We focus on three main models, one case where the dipole magnetic moments in both neutron stars are aligned, another where they are anti-aligned and one where the two dipoles are aligned but with one dipole having a maximum strength smaller by two orders of magnitude. Our goal is to systematically study the major differences in the evolution and the overall energetics of the emitted EM bursts. In the first two cases, the magnetic field is of the same order of magnitude in both stars. We discuss the similarities of these cases with the gravitational collapse of a single neutron star [Most et al. \(2018\)](#); [Nathanail et al. \(2017\)](#). We follow the evolution after BH formation until the EM fields decay to insignificant values, and further set limits on the expected flux that would be detected from a BNS merger that promptly collapsed to a BH with similar properties and distance to GW190425 ([The LIGO Scientific Collaboration et al. 2020](#)).

It has been proposed that NS mergers may give rise to fast radio bursts (FRBs) ([Lasky et al. 2014](#); [Zhang 2016](#); [Wang et al. 2016](#); [Metzger & Zivancev 2016](#); [Piro et al. 2017](#)). In this study we state the proposition that FRBs can be related to neutron star mergers only in the case that the remnant undergoes a prompt collapse to a BH ([Paschalidis & Ruiz 2018](#); [Nathanail 2018](#)). The simulations we study show that in the case of a negligible disk around the remnant BH, the magnetic field dissipates and produces giant EM pulses. In this study we do not model the last orbits of a quasi-circular binary, but rather restrict only to the collision. We believe that these results can be considered as a toy model that can give an illustrative picture of the EM pulses expected from a prompt collapse to a BH.

This paper is organized as follows: in Sec. 2 we review the numerical setup of the simulations together with the initial data. In Sec. 3 we present the numerical results and the comparison between the various models. In Sec. 4 the astrophysical relevance of pair production and magnetic reconnection is discussed, whereas the luminosity and the observable limits are left for Sec. 5. Finally, the discussion and the conclusions of our results are presented in Sec. 6.

## 2. NUMERICAL SETUP AND INITIAL DATA

All simulations presented in this paper have been performed using the general-relativistic resistive magneto-hydrodynamics (GRMHD) code

*Software:* resistive WhiskyRMHD ([Dionysopoulou et al. 2013, 2015](#)) embedded in the

*Software:* Einstein Toolkit ([Löffler et al. 2012](#)) and box-in-box mesh refinement is provided by

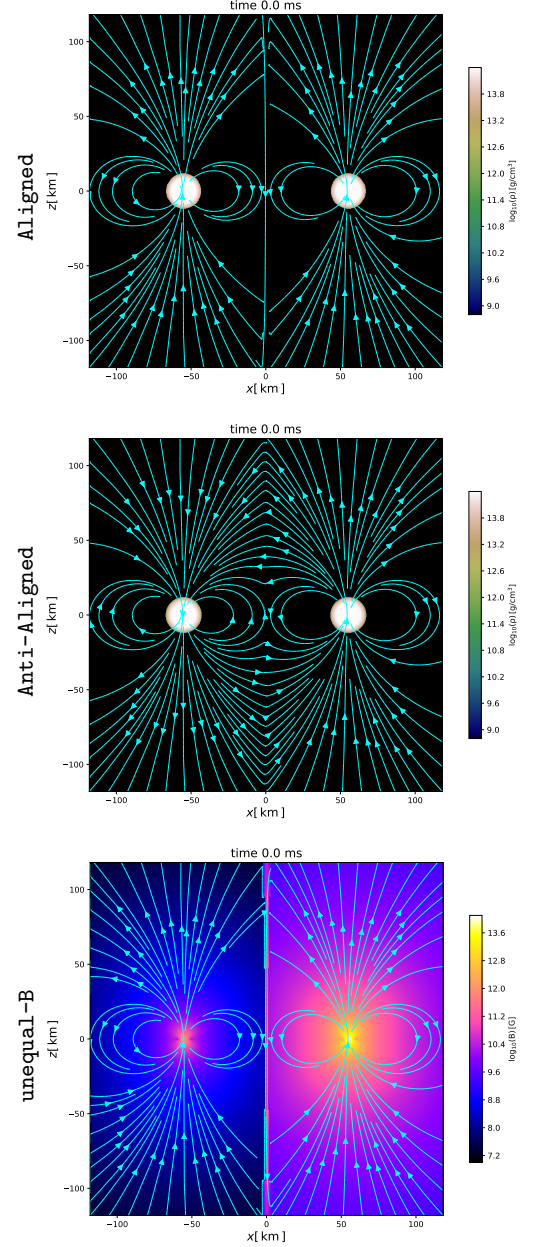


**Figure 1:** Magnetic field configuration at the initial time, upper panel: the rest-mass density for model **A1<sub>1</sub>**, middle panel: the rest-mass density for model **Anti-a1<sub>1</sub>** and lower panel: the magnetic field strength for model **unequal-B**, is depicted since the density profile and magnetic field lines are the same as in the upper panel.

*Software:* Carpet, where initially tracks the two stars ([Schnetter et al. 2004](#)). The numerical setup is similar to the one presented in [Nathanail et al. \(2017\)](#); [Most et al. \(2018\)](#). The GRMHD equations are solved using high-resolution shock capturing methods like an LLF Riemann solver and the reconstruction of the primitives is done by enhanced piecewise parabolic method (ePPM) ([Colella & Sekora 2008](#); [Reisswig et al. 2013](#)). The elec-

tric charge is not evolved but computed from  $q = \nabla_i E^i$  at every timestep, similar to [Dionysopoulou et al. \(2013\)](#) and [Bucciantini & Del Zanna \(2013\)](#).

The focus of our study is the magnetic field structure and the produced luminosity after the collision in which a BH is formed. We assume that the two stars have neutral magnetospheres, i.e., no charge density exists and no currents will develop in the exterior magnetospheres, and hence model them in electrovacuum. The use of an ideal-MHD framework is sufficient to describe a BNS merger ([Harutyunyan et al. 2018](#)), but not the evolution of the magnetosphere. In such cases we need to solve the Maxwell equations in the exterior in electrovacuum, which can be achieved through a resistive-MHD framework. The goal of this approach is the inclusion of an electric current that recovers the ideal-MHD limit inside the star and the electrovacuum limit outside, which is filled by a low density zero-velocity atmosphere, which then decouples from the evolution of the EM fields. Due to the small timescales associated with the ideal-MHD current the GRMHD equations can become quite stiff in this limit. In order to allow for a numerically stable treatment of these regions we employ an implicit-explicit Runge-Kutta time stepping (RKIMEX) ([Pareschi & Russo 2005](#)). For further details of our numerical setup we refer to [Dionysopoulou et al. \(2013\)](#), [Dionysopoulou et al. \(2015\)](#) and [Palenzuela \(2013\)](#).

To accommodate changes in the space-time due to the motion of the two neutron stars the metric is evolved in the CCZ4 formulation [Alic et al. \(2012, 2013\)](#) as implemented by the

*Software:* McLachlan code ([Löffler et al. 2012](#)). One feature of this formulation is the inclusion of constraint damping terms [Gundlach et al. \(2005\)](#) which can suppress violations of the Einstein equations and thus improve numerical stability [Alic et al. \(2013\)](#).

This is of particular importance to our choice of initial data. Previous studies of head on collisions in pure hydrodynamics have either resolved the constraint equations [Paschalidis et al. \(2011\)](#) or have superimposed two TOVs solved in isolation far enough apart in order to minimize violations [Kellerman et al. \(2010\)](#); [Rezzolla & Takami \(2013\)](#). In this study, we use the constraint damping terms in the evolution scheme to remove inconsistencies in the space-time variables of our initial data. Such an approach is in line with studies of spinning neutron stars in binary systems [Kastaun et al. \(2013, 2016a\)](#) or studies of eccentric encounters of binary neutron stars [Radice et al. \(2016\)](#); [Papenfort et al. \(2018\)](#).

Accordingly, we consider two neutron stars separated by 110 km along the  $x$ -axis. They are initially endowed with a dipole magnetic field extending also to the exterior of the two stars. The phi component of the vector

potential,  $A_\phi$ , that we use to generate the dipole field is given below ([Shibata et al. 2011](#)):

$$A_\phi = \frac{A_b r_d / \sqrt{2}}{\sqrt[3]{(x^2 + y^2 + z^2 + 1/2 r_d^2)}}, \quad (1)$$

where  $r_d$  is the radius of the current loop that generates the dipole and  $A_b$  is a scaling factor that determines the strength of the field. We consider two different cases for the magnetic field initial geometry, one where both dipoles are aligned with respect to each other and the symmetry plane ( $y - z$ ) and another where one dipole is anti-aligned with the other. Notice that by changing the sign of the vector potential we get the anti-aligned magnetic field. Every magnetosphere occupies the half domain and there is a mismatch exactly at the  $y - z$  plane, which passes through the origin. The reason why we choose this configuration, is to allow for an initial readjustment of the magnetospheres as the evolution begins, instead of an initial superposition of the two dipoles. The choice we make results in an initial peak in radiation, analogous to the so-called "junk radiation", which quickly reduces to two orders of magnitude, before the actual burst from merger is detected, this is discussed with the presentation of fig. 8. The neutron stars have an initial separation of 110 km, in order to allow for the impact of the initial "junk radiation" to decrease significantly (two orders of magnitude in luminosity), before the main EM emission is produced by the merger itself. Furthermore notice that due to the lack of a quasi-circular orbit, the merger occurs in less than a ms. The initial configuration can be seen in fig. 1 where we plot the magnetic field lines at the initial setup for the three representative models.

Our numerical domain consists of six refinement boxes, where the resolution doubles when going to the next higher refinement level. The outer boundary is placed at  $\sim 378$  km. As the two stars move towards each other, the finest resolution is  $\Delta x \sim 367$  m. At the time of merger, where the collapse is triggered, an extra refinement level is added making the highest resolution  $\Delta x \sim 183$  m, note that this is considerably higher than the one used in [Palenzuela et al. \(2013b\)](#). In order to check the robustness of our results with respect to resolution, we run an extra simulation, model **Anti-AL<sub>1</sub>, high-res.** with the finest resolution at  $\Delta x \sim 294$  m, which at the time merger becomes  $\Delta x \sim 147$  m.

The neutron stars are modeled as non-rotating. We have considered a simple polytrope with  $\Gamma = 2$  and  $K = 100$  which for a gravitational mass of  $M = 1.4M_\odot$  yields a radius  $R_{NS} = 11.94$  km and central density of  $\rho_c = 7.92 \times 10^{14}$  g/cm<sup>3</sup>. The choice of equation of state in this study is not so relevant, since our focus is on the EM pulses produced by the magnetic field which decouples



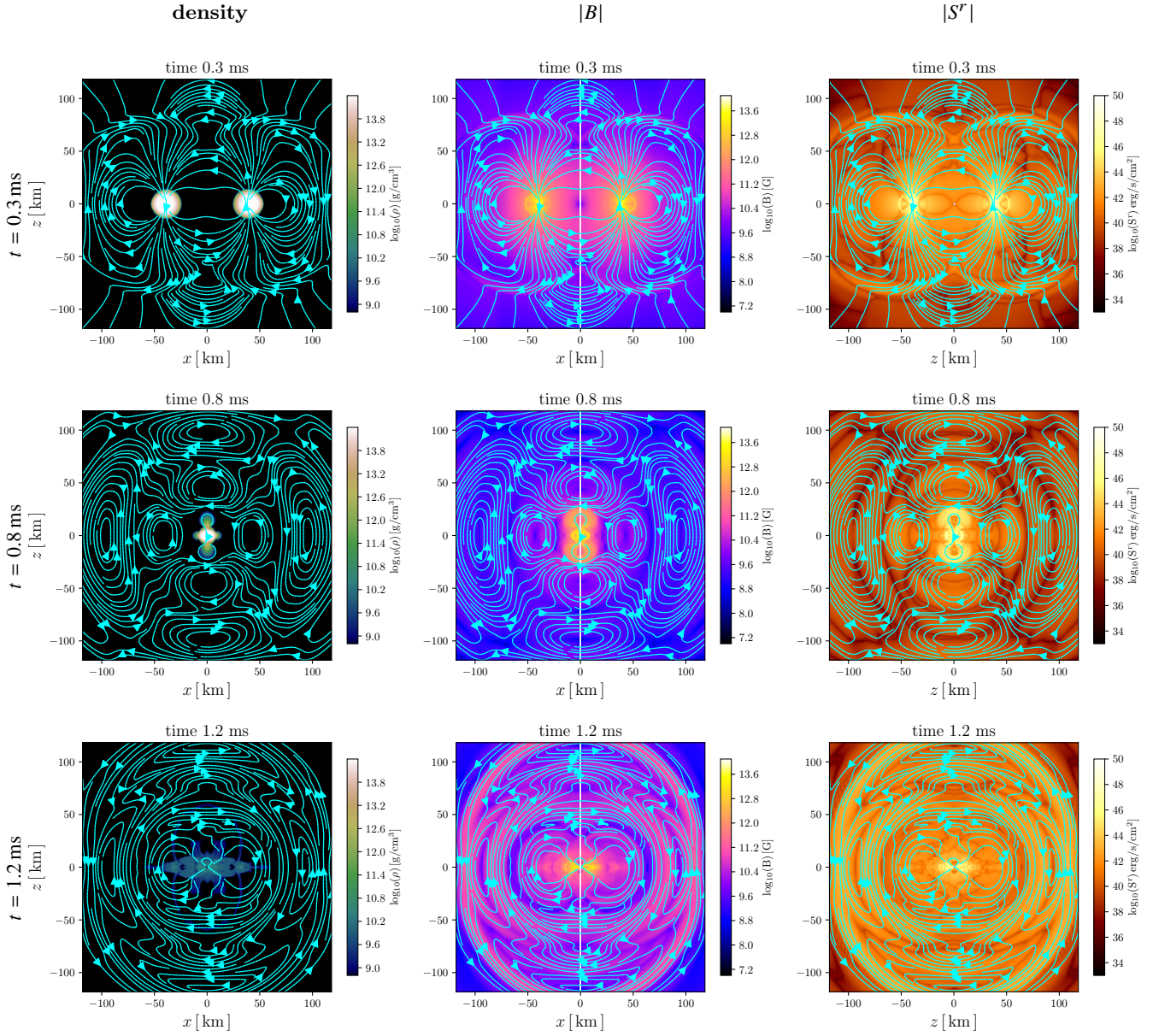


**Figure 2:** Anti-aligned case **Anti-a1<sub>1</sub>**. From left to right: evolution of the density, magnetic field strength and the radial component of the poynting vector  $S^r$ . The different rows correspond to different times  $t = 0.3, 0.8$  and  $1.2$  ms.

from the fluid and dissipates away. Both stars have an initial velocity  $v^x \simeq 0.15c$ , moving on the  $x$ -axis towards each other.

### 3. NUMERICAL RESULTS

In this section we will present and describe the results of our numerical simulations for the head on collision of two magnetised neutron stars for six different cases, which are briefly described in Table 1. The differences in the models used in this study are purely in the magnetic field configuration. All the hydro-dynamical properties of the stars are the same in all runs. The different magnetic field configurations are as follows: four cases for two aligned dipoles with the same maximum magnetic

field strength, which ranges  $B_{\max} \simeq 10^{12}, 10^{13}, 10^{14}$  and  $10^{15}$  G respectively and one case where the two magnetic fields differ by two orders of magnitude, namely the one star has  $B_{\max} \simeq 10^{14}$  G and the other  $B_{\max} \simeq 10^{12}$  G. And lastly, two cases with anti-aligned magnetic dipoles with magnitude of  $B_{\max} \simeq 10^{13}$  and  $10^{14}$  G respectively. The reason to choose four different magnetic field strengths for a single model is to acquire and test the expected relation between magnetic field strength and luminosity, further note that since the density scaling in numerical relativity simulations is tied by the construction of the neutron star, every such simulation has a different value for the plasma beta parameter inside the star,  $\beta = p/p_m$  (fluid pressure  $p$  over magnetic pressure  $p_m$ ). This scaling

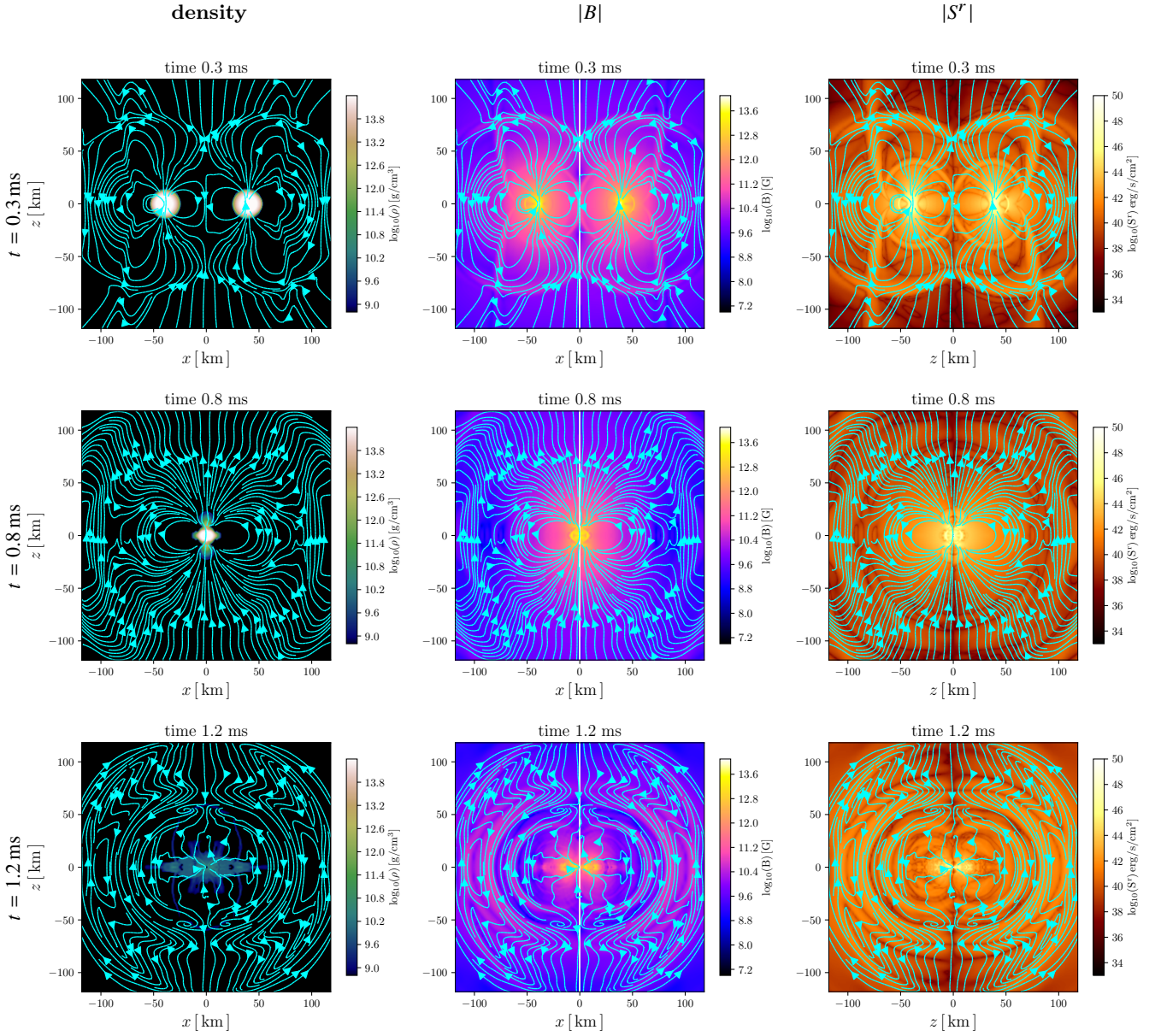


**Figure 3:** Aligned case A1<sub>1</sub>. From left to right: evolution of the density, magnetic field strength and the radial component of the poynting vector  $S^r$ . The different rows correspond to different times  $t = 0.3, 0.8$  and  $1.2$  ms.

is discussed and recovered in Sec. 5, and thus the results from the other models can be extrapolated according to this scaling, for different magnetic field strengths.

The matter and space-time dynamics in a head-on collision of two NS have been studied in detail (Kellerman et al. 2010; East & Pretorius 2013; Rezzolla & Takami 2013). We only sketch briefly the evolution of the matter which is essentially identical in all cases. The two NS move towards each other with an initial velocity of  $v^x \approx 0.15c$ . The two stars touch at time  $t_{\text{merge}} \approx 0.58$  ms, an apparent horizon is found for the first time at  $t_{\text{BH}} \approx 0.81$  ms (fig. 2 and 3) and the bulk of the matter has already crossed the horizon by  $t \approx 1.7$  ms.

The first case that will be described is the one where

initially the two NS are endowed with a dipolar field anti-aligned with respect to each other, model **Anti-a1<sub>1</sub>**. When the stars start to move, the two magnetospheres begin to interact. The opposite field components cancel out and the field lines reconnect, as can be seen in the first row of fig. 2. As both stars come closer this structure evolves to a quadrupolar-like field (second row fig. 2). On both sides right and left the dipole field of each star is still well structured and with different polarity with respect to each other.

At the time of merger ( $t \approx 0.58$  ms) these magnetic-loop structures are still anchored on the stellar matter. Quickly after the two stars merge, the magnetic-loop structure is disengaged from the matter and radi-



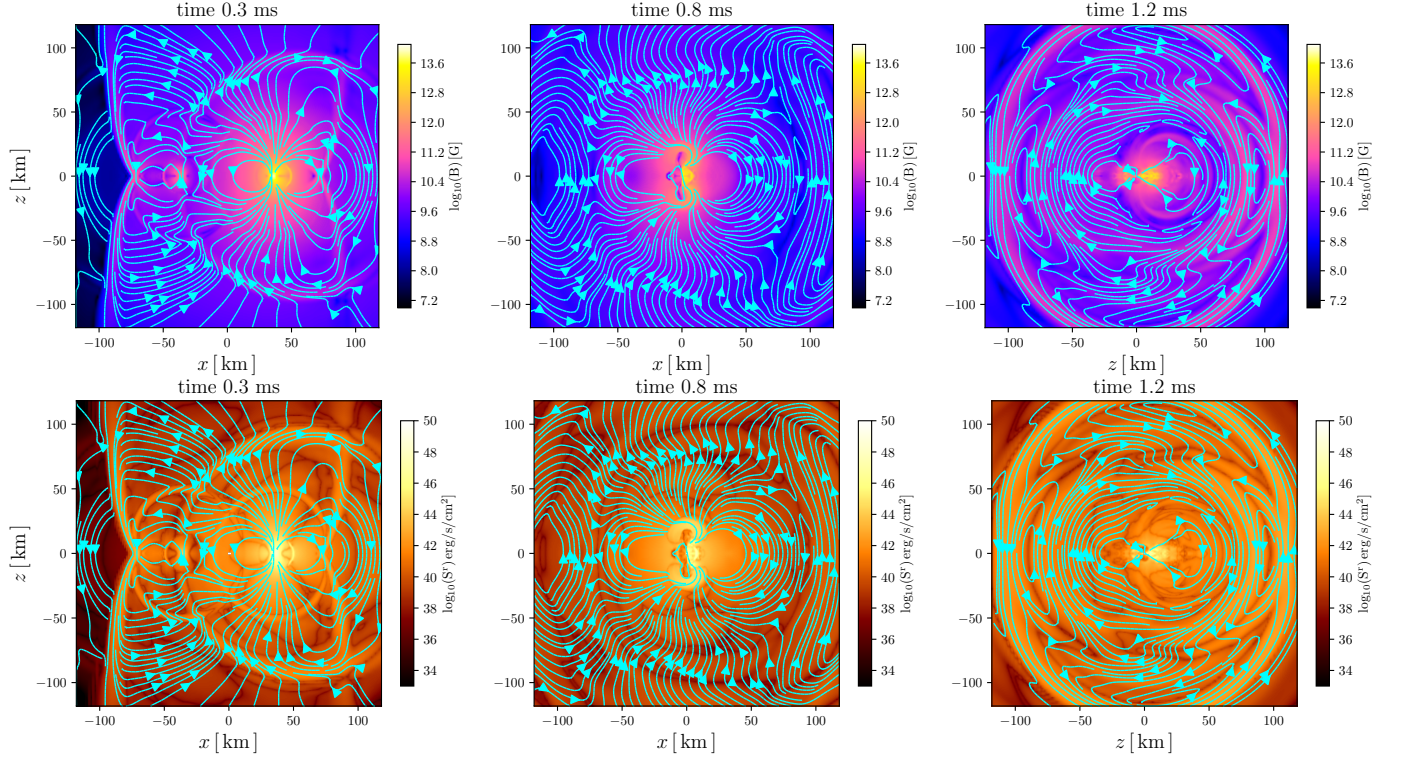


**Figure 4:** For the unequal magnetic field case, evolution of the magnetic field strength (upper panels) and the radial component of the poynting vector  $S^r$  (lower panels), in the two rows respectively. The different columns correspond to different times at  $t = 0.3, 0.8$  and  $1.2$  ms.

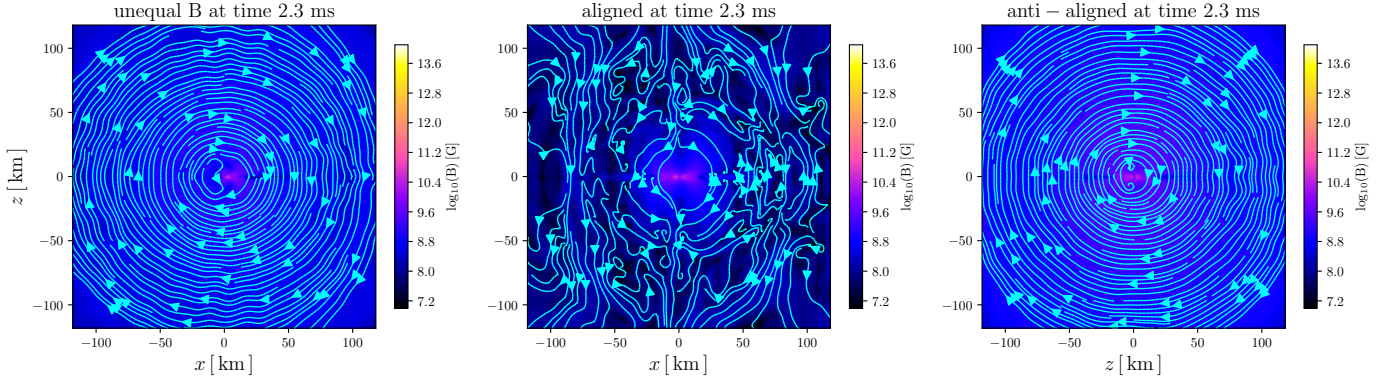


**Figure 5:** Magnetic field strength for for three different models at late time  $t = 2.2$  sec. From left to right is the unequal B (*unequal - B*), aligned ( $AI_1$ ) and anti-aligned (*Anti - al1*) case respectively. The maximum magnetic field strength in the vicinity of the BH is less than  $10^9 G$ .

ated away. As can be seen in the second row of fig. 2, this is produced during merger and subsequently radiated away following the third row of fig. 2. This EM pattern is evident when looking at the radial component of the poynting vector ( $S^r$ , third column in fig. 2 and 3).

After that, the explosion has a spherical shape with an excess of energy radiated towards the equator. The formed BH, following the collision of the two stars, continues to ring down as it settles down. This continuously

distorts the magnetic field at the vicinity of the BH producing more pulses with less intensity. At time  $\sim 1.6$  ms the magnetic field strength around the BH is less than  $10^{10} G$  and continuous to decay. The loop structure of the magnetic field is still being distorted by the settling of the BH.

The second case that we study, is the one with both dipoles aligned and parallel to the  $z$ -axis (model  $AI_1$ , from Table 1). As before, each dipole is extended and filling

the half space depending on where the neutron star is placed, right or left of the  $y - z$  plane. When the simulation starts both dipoles meet exactly at this plane. A small shock is induced to both magnetospheres as the two stars start to move (first row of fig. 3), which is analogous to the “junk radiation” reported in the literature. Note that this initial transient reduces significantly, before the burst from merger is detected. As the two stars are ready to merge, the magnetic structure resembles that of a big dipole (second row of fig. 3). The continuation of this model closely resembles the collapse of a massive neutron star (Most et al. 2018). After merge, the apparent horizon is formed and the field lines are violently snapped as the highly conducting matter hides behind the horizon. During this, quadrupolar EM radiation is generated and propagates outwards. This quadrupolar pattern is the main difference from the anti-aligned case, where the EM radiation is mostly spherical at this stage. In the last phase, when the bulk of the matter is already behind the horizon, the radiation pattern follows the ringing down of the BH, we will come again to this point when analyzing the EM pulses.

The next case we discuss is the model *unequal - B*, where the two NSs have aligned magnetic dipoles with a two orders of magnitude difference in strength, this model is the most likely relevant for astrophysically realistic conditions. In the initial phase of this run, the magnetosphere of the high-field NS (which is the one on the positive part of the x-axis 4) quickly engulfs the magnetosphere of the low-field NS. This acts as a slight shock to the magnetosphere of the high-field NS. At the time of merger and after that, the EM radiation follows a similar pattern with that of model *AI<sub>1</sub>*, the main difference is that the right (undistorted) side is more efficient in radiation as can be seen in the third column of fig. 4. The main features of the magnetic field follow the evolution of the high field magnetosphere, whereas the other NS acts as a simple companion star, introducing a large perturbation to the overall magnetospheric structure. Due to the resistivity of the secondary neutron star (the one with the lower magnetic field), the magnetic field lines are anchored on the surface of the star (left panel of fig. 4). However, after merger the evolution of the EM field is dictated by the matter dynamics and the produced magnetic loops are generated similarly to model *Anti-al<sub>1</sub>* (third column of fig. 2 and 4).

It is interesting to see what is left around the BH at late times ( $t \simeq 2.3\text{ms}$ ). The case with the initial aligned dipoles (*AI<sub>1</sub>*) closely compares with the collapse of one massive magnetised NS (middle panel of fig. 5, compare with Most et al. (2018)). For the other two cases, the anti-aligned dipoles and the unequal magnetic field, the late time evolution is similar, making a bubble-like structure around the BH. At such late times the strength

of the magnetic field, in the vicinity of the BH, is less than  $\sim 10^{11}\text{G}$ . It is important to check and discuss the physical mechanism of pair creation and magnetic reconnection in this numerical setup, as these are expected to happen similarly with pulsar magnetospheres.

#### 4. PAIR PRODUCTION, MAGNETIC RECONNECTION AND HIGH ENERGY RADIATION

Before computing the EM output from the the models described in this study, we focus in the efficiency of pair production during such cataclysmic events. Moreover, we follow regions where this may occur and regions of magnetic field alternating polarity that reconnection is expected in a realistic environment.

One of the dominant mechanisms for pair creation in a pulsar magnetosphere is the interaction of high energy (usually curvature photons) with strong magnetic field. The important ingredient for this mechanism to start to operate is a strong electric field component parallel to the magnetic field. In this section we discuss the occurrence of the physical conditions that would trigger pair creation during an event similar to the ones described in these simulations. The initial conditions that we employ have an empty of charges environment around the two neutron stars. During the simulation high electric field is generated which we follow in order to check where the condition of pair creation is met.

Due to the developed voltage drop  $\Delta V$ , a charge attain a Lorentz factor  $\gamma$ , which is given by

$$\gamma = e \Delta V / m_e c^2, \quad (2)$$

where  $e$  and  $m_e$  is the electric charge and the mass of the electron, respectively.

The condition for pair creation is given as follows: (Sturrock 1971; Ruderman & Sutherland 1975)

$$\gamma^3 \left( \frac{\hbar c}{2m_e r_c c^2} \sin \theta \right) \left( \frac{B_{\text{loc}}}{B_{\text{cr}}} \right) \simeq \frac{1}{15}, \quad (3)$$

where  $B_{\text{loc}}$  is the local magnetic field,  $B_{\text{cr}} := 4.4 \times 10^{13}\text{G}$  is the so-called critical magnetic-field strength and  $\sin(\theta)$  is the “pitch” angle between the photon and the magnetic-field line.  $r_c$  is the radius of curvature of the magnetic-field line that the charge will travel on. Using the above mentioned equations, we report the criterion for triggering pair creation

$$E < E_{\text{pp}} \simeq 1.5 \times 10^{11} \left( \frac{r_c}{20\text{km}} \right)^{2/3} \left( \frac{B_{\text{loc}}}{10^{10}\text{G}} \right)^{-1/3} \text{statV/cm}. \quad (4)$$

In order to evaluate the occurrence of pair creation in the cataclysmic environment of colliding neutron stars, we report the strength of the parallel electric field  $E_{\parallel} :=$



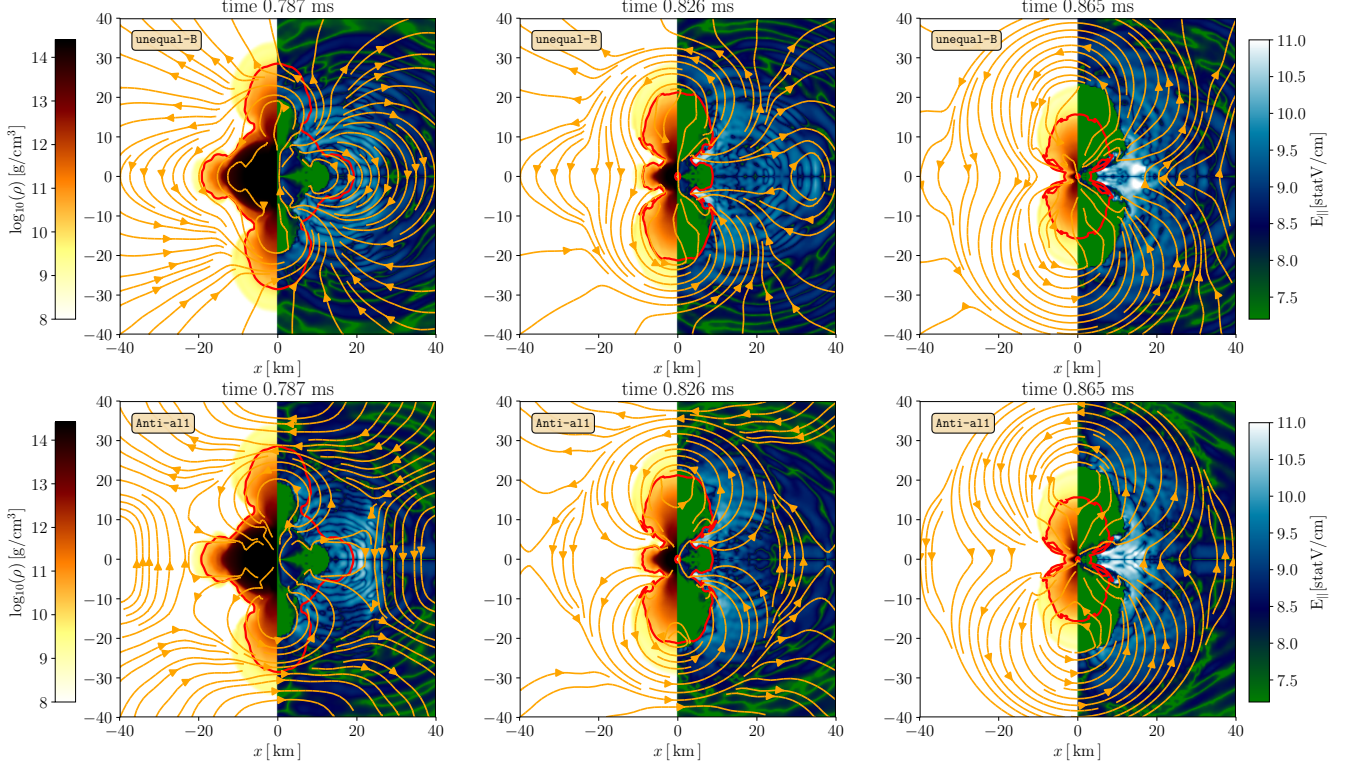


**Figure 6:** Upper panels: *unequal-B*, lower panels: *Anti-al<sub>1</sub>*. Left plots show rest-mass density, whereas the right plots show the electric field parallel to the magnetic field, both in the  $(x, z)$  plane shown at three different times. Also reported are the stellar surface (solid red line) and the magnetic-field lines (orange lines).

$\mathbf{E} \cdot \mathbf{B} / |\mathbf{B}|$ . The models under investigation are *unequal-B*, where the two stars have an unequal initial magnetic field and *Anti-al<sub>1</sub>*, initial magnetic dipoles are anti-aligned.

In fig. 6 we show for these two models, the evolution of the rest-mass density (left panels) and the parallel electric field (right panels) at three representative times, at which  $\mathbf{E}_{\parallel}$  reaches a rather high value. Also shown in fig. 6 are the stellar surface (solid red line) and the magnetic-field lines (orange lines).

Note that initially, for model *unequal-B* (upper panels) the neutron star with the higher magnetic field is placed on the positive  $x$ -axis, which means it is on the right side of the figures. This is the reason of the asymmetry of the magnetic field lines as can be seen in all panels. This is also imprinted in the development of the parallel electric field where on the right side it reaches the highest values, whereas on the left it retains low values at all times. As a result pair creation would be expected in a neutron star head on collision, if one of the two stars has the limiting initial magnetic field of  $B_{\text{pol}} = 10^{13}$  G, lower values would most probably suppress pair creation.

For model *Anti-al<sub>1</sub>* (lower panels of fig. 6), a similar situation with model *unequal-B* is depicted, high values of electric field are generated at regions where the magnetic field is changing polarity (visible in all three

panels). Matter dynamics, during merger and close to the collapse to a BH, twist the magnetic field lines generating an enormous electric field in the region where magnetic reconnection is expected. In the middle and rightmost plots of the lower panels of fig. 4, at the left part of the plots near the equatorial plane, it is seen that the magnetic field is changing polarity and exactly at this place a huge parallel electric field is developed. From our simulations we can extract these estimates for the strength of the developed parallel electric field, since we allow regions with  $B^2 - E^2 < 0$  to develop. This is also illustrated in fig. 7 where we plot the quantity  $B^2 - E^2$  in a logarithmic scale, but also incorporating the sign of it, to better understand these regions where electric fields develop and magnetic reconnection is expected in a realistic environment. Regions of magnetic field alternating polarity can be observed at the interfaces of magnetic loops with different orientation, in fig. 7 these are located on a circle of radius  $\sim 100$  km. Moreover, similar regions of alternating magnetic field polarity are observed on the equatorial plane from  $\sim 50$  km till the star surface, which are seen in fig. 7.

In our simulations the EM field energy is carried away by these huge magnetic loops described above, these magnetic loops are generated from the merger of the

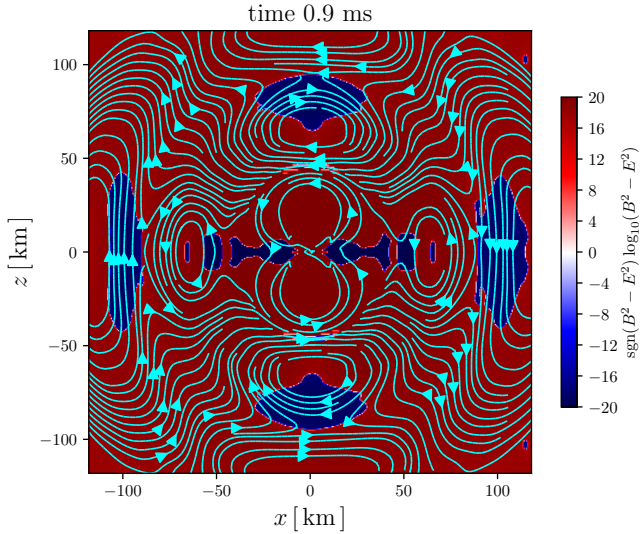


**Figure 7:** The logarithm of  $B^2 - E^2$  multiplied by its sign, to account for negative values, in the  $(x, z)$  plane shown at time  $t = 0.9$  ms for model *Anti-a1*. Red regions indicate magnetically dominated regions, whereas blue regions electrically dominated regions which are allowed to develop with our numerical scheme. It is exactly at the interface of these two regions that magnetic reconnection is expected and could provide energy dissipation and high energy radiation.

two magnetospheres and are further influenced by the dynamics of the matter, which after merger have this bubble shape shown in the left-part of all plots in fig. 6. The magnetic bubbles that are produced, move outwards in all directions, from the equatorial plane to the north and south, and let us estimate the magnetic energy dissipated after merger. Under the conventions of the numerical scheme used in our simulations no dissipation can be modeled locally, but only a global picture can be drawn, of the magnetic energy that escapes after merger in the form of Poynting flux. As such, the estimations derived in the next section can be regarded as rough limits of the emission produced from a BNS merger that undergoes a prompt collapse.

## 5. ELECTROMAGNETIC OUTPUT

In this section we will discuss the EM emission of all the head on collisions performed in this study. While we are interested in giving an estimate of the radiated energy we also track the pattern of the EM pulses produced during such collisions. We compute the EM luminosity as:

$$L_{\text{EM}} = \oint_{r=\text{const}} T_{\text{EM}}^t r \, d\Omega \quad (5)$$

on a surface at  $r \simeq 220.5$  km from the merger site of the two neutron stars. Before the two stars merge, the EM signal is dominated by an early transient as the two stars

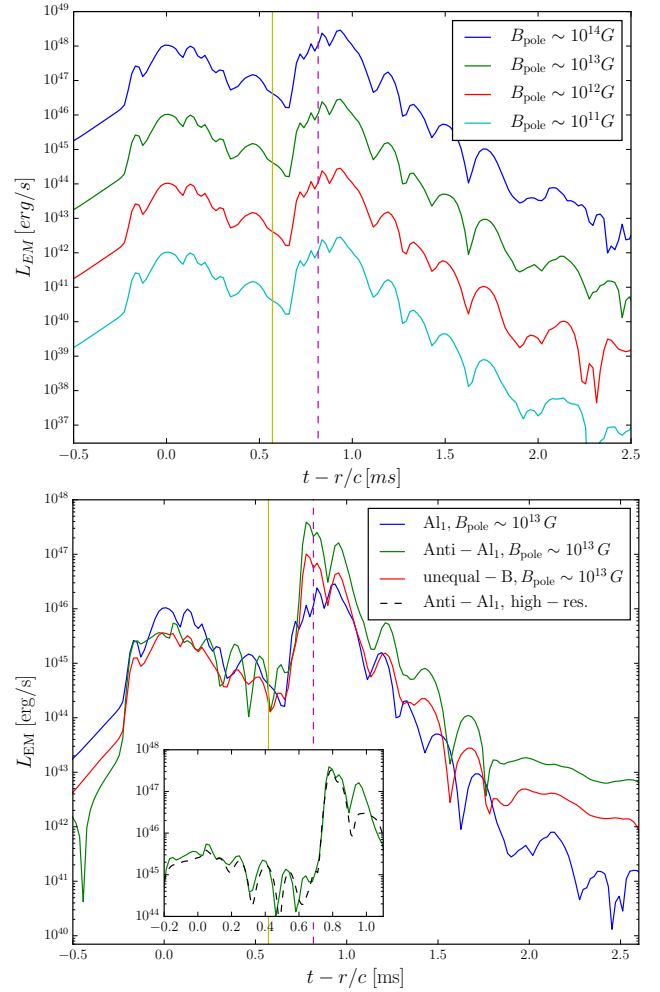


**Figure 8:** EM luminosity is extracted at 220.5 km, and expressed in retarded time, for models, upper panel: *Al1*, *Al2*, *Al3* and *Al4*, lower panel: *Anti - a1*, *unequal - B* and *Al1*. The solid yellow line represents the time of merger and the dashed magenta line the time when the apparent horizon is found for the first time. The maximum magnetic field of each model is stated inside the plots. In the embedded plot the *Anti - a1* high resolution run is compared with the base resolution.

start to move towards each other, the “junk radiation” already discussed. This transient is the result of our ad-hoc placement of the initial dipole magnetic fields that initially have to adapt to our prescription for the resistive surface layer of the two stars (Dionysopoulou et al. 2013). While EM outflows are expected from the quasi-circular orbital motion of realistic binaries (Hansen & Lyutikov 2001; Lai 2012; Piro 2012), the transient found here is a pure numerical artifact that, however, due to similar energetics is of similar magnitude to that expected for realistic BNS.

At the time of merger the compression of the two magnetospheres leads to a strong peak in the luminosity peak,

see fig. 8 which is shown in retarded time to account for the time delay to reach the detector. At the time the actual burst is detected, the radiation from the initial transient, the “junk radiation” depicted at 0 ms, has decreased almost two orders of magnitude, this gives us confidence that the main luminosity peak is not affected by this. It is important to note that the luminosity is increased in the anti-aligned case compared to the aligned case, whereas the unequal magnetic field configuration lies in between the other two. We speculate that this may be due to the alternating magnetic polarity close to the surface of the two stars. A similar behavior was also found in the inspiral of two neutron stars with their magnetospheres evolved in a highly conducting medium (Palenzuela et al. 2013b). The EM luminosity reported here is expected to be similar with the one from a prompt collapse after a BNS merger, however two points need to be made here, firstly the magnitude of the expected luminosity compared with what we find may be overestimated, since dissipation from magnetic reconnection via current sheets may reduce the magnetic energy, second this dissipated magnetic energy in current sheets can be a source of high energy radiation potentially observable when a BNS merger remnant undergoes a prompt collapse to a BH, this is something that we further discuss in fig. 10.

In all three cases after the merger the signal and the EM fields decay rapidly. This is not surprising since a non-spinning BH is formed, which cannot support a stationary magnetic field configuration, unlike for spinning BHs where a Kerr-Newman BH can be formed (Nathanail et al. 2017). At merger a transient is formed, which depends on the precise distortion of the magnetospheres and the space time. After a BH has formed it will ring down to a stationary Schwarzschild solution and consequently the imprint of the quasi-normal modes of the BH are also found in the decaying magnetic field, much like in the gravitational wave signal. A similar feature has been observed and studied in previous simulations of collapsing magnetized neutron stars with electrovacuum magnetospheres (Most et al. 2018; Dionysopoulou et al. 2013; Baumgarte & Shapiro 2002).

Next, we compute the overall emitted EM energy during these events. The goal is to provide an analytic description of the radiated energy in terms of magnetic field strength and the corresponding efficiency in terms of the initial magnetic field orientation, in analogy to the case of single star collapse (Most et al. 2018). Accordingly, we compute the EM energy as:

$$E_{\text{EM}} := \int L_{\text{EM}}(t) dt, \quad (6)$$

and report it in Table 1 for all different initial configurations. Similar to what was found for collapsing isolated

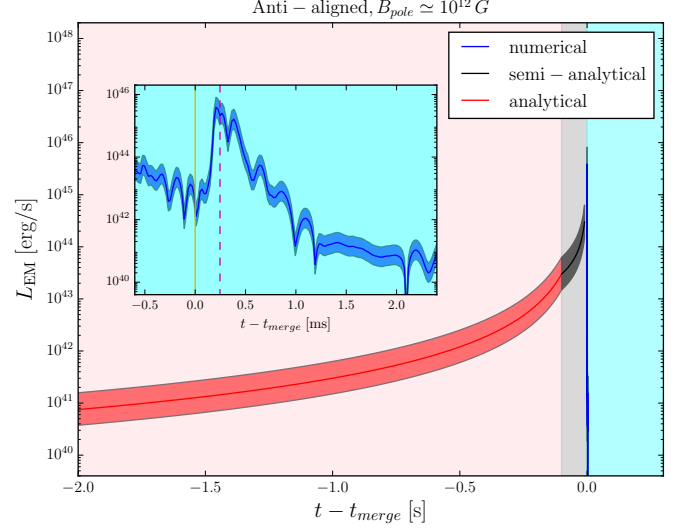


**Figure 9:** EM luminosity for the **Anti- $Al_2$**  model. Zoom-in panel: the numerical lightcurve, the solid yellow line represents the time of merger and the dashed magenta line the time when the apparent horizon is found for the first time. Big panel: the precursor signal is reproduced by Eq. (9) till one hundred milliseconds before merger, then for the last hundred milliseconds the scaling  $L_{\text{EM}} \propto \Omega^{3/2}$ , where  $\Omega$  is the orbital frequency of the binary, is used. After merger the signal is the output of our numerical simulation. It mimics the expected EM signature from a quasi-circular binary that undergoes a prompt collapse in 0.5ms.

neutron stars (Most et al. 2018), we observe a perfect  $B^2$  dependency of the energy as expected on dimensional grounds (fig. 8, upper panel).

The reason to run all these models  $Al_1$ ,  $Al_2$ ,  $Al_3$  and  $Al_4$ , is to test the dependence of the luminosity with the initial magnetic field strength in the range of  $\sim 10^{11} - 10^{14}$  G (for the initial magnetic field at the pole), and then use this scaling to extrapolate also for the other models in the same range<sup>1</sup>. We find an almost perfect  $\propto B^2$  scaling that holds in this range, with even the smallest features on the lightcurve being identical in all four cases. This gives us confidence that the results of all other models can be safely extrapolated in this range of magnetic field strengths. In the embedded plot we present the comparison with the high resolution run for model **Anti- $Al_1$** , the main peak of the lightcurve, that carries most of the energy, is in good agreement both in terms of energy and the time when the peak occurs.

In order to quantify the main differences of the emission efficiency due to the various initial magnetic field configurations, we estimate the available power in the

<sup>1</sup> As discussed in Sec. 3, the initial plasma parameter  $\beta$  inside the stars is different for different initial magnetic field strength of the neutron stars, so the magnetic field scaling needs to be tested.



two magnetospheres using a modified version of the phenomenological expression proposed by [Falcke & Rezzolla \(2014\)](#).

$$P_{\text{MS}} \simeq 16.8 \times 10^{44} \eta_{\text{B}} t_{\text{ms}}^{-1} b_{12}^2 \text{ erg s}^{-1}, \quad (7)$$

where  $\eta_{\text{B}}$  is the EM efficiency, the fraction of the dissipated magnetic energy,  $\Delta t = t_{\text{ms}}$  ms is the duration of the peak in the luminosity curve, while  $b_{12}$  is the polar magnetic field of the star in units of  $10^{12}$  G. Notice, that here we report the polar value and not the maximum magnetic field, in order to allow for straight comparisons with the respective magnetic efficiency from single collapsing NS.

In all models the burst-like high luminosity peak is of the order of one millisecond, thus  $\Delta t_{\text{EM}}/\text{ms} = 1 = t_{\text{ms}}$ . The emitted energy can be expressed as:

$$E_{\text{EM}} = P_{\text{MS}} \Delta t_{\text{EM}} \simeq 16.8 \times 10^{41} \eta_{\text{B}} b_{12}^2 \text{ erg}. \quad (8)$$

The duration of these burst-like peaks in luminosity is dictated by the matter dynamics and the almost immediate collapse to a BH, this is the reason why the simulations described here, can be regarded as a toy model for BNS mergers that promptly collapse to a BH, since the head-on collision is not related to any of the features on the luminosity lightcurve. From the radiated energy for the different models in Table 1 and expression 8, we can deduce the magnetic efficiency  $\eta_{\text{B}}$ . For the three models with the different magnetic field initial configuration we find: for **Anti-al<sub>1</sub>**  $\eta_{\text{B}} \simeq 12\%$ , for **unequal-B**  $\eta_{\text{B}} \simeq 3.7\%$  and **Al<sub>1</sub>**  $\eta_{\text{B}} \simeq 2\%$ . Several important remarks can be made here. As we followed the evolution of the **Al<sub>1</sub>** model in Sec. 2, where both magnetic dipoles are initially aligned, we argued that after merger the evolution closely mimics that of a collapsing magnetised NS. It was found that the mean magnetic efficiency from such a collapse is  $\eta_{\text{B}} \simeq 2\%$  ([Most et al. 2018](#)), which is exactly what we get for the aligned case. In the case with unequal magnetic field, the efficiency is almost twice higher and in the most efficient magnetic field configuration, the anti-aligned dipoles, the efficiency is six times higher than the aligned one.

The computed estimates for the radiated energy and luminosity, together with the luminosity curves of fig. 8, point that the EM energy radiated in such events can potentially be compared with the phenomenology of FRBs (for a review [Rane & Lorimer \(2017\)](#)). Although the systems studied in this work are highly idealised and merely serve as a toy model to investigate a prompt collapse scenario, we can still draw qualitative conclusions relevant for realistic BNS configurations. In particular BNS systems with very high masses are known to undergo a prompt collapse ([Hotokezaka et al. 2011](#); [Bauswein et al. 2013](#); [Ruiz & Shapiro 2017](#); [Köppel et al. 2019](#)), where a light disk is formed ([Nathanail 2018](#); [Paschalidis & Ruiz](#)

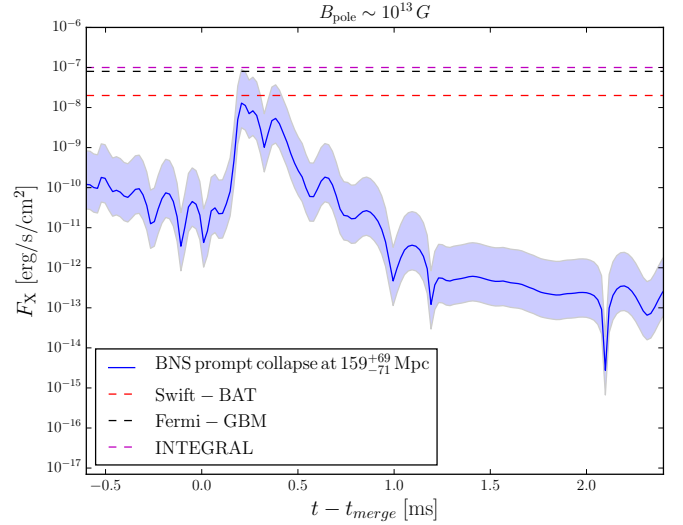


**Figure 10:** Estimated flux from a BNS that promptly collapsed to a BH at a distance of  $159^{+69}_{-71}$  Mpc, with shaded blue the upper and lower limits for the flux. The dashed lines correspond to the flux limits of satellites that look blindly for burst-like events, (dashed red) *Swift* (BAT) 15–100 keV, (dashed black) *Fermi* (GBM) 20 keV–40 MeV and (dashed magenta) *INTEGRAL* (IBAS) 20–200 keV, where we have converted their photon rate in their respective energy band, into observed flux.

[2018](#)). The lifetime of this disk is found to be of the order of milliseconds ([Ruiz & Shapiro 2017](#)). Thus, the disk will not be able to keep the magnetic field from dissipating and a large fraction of the magnetic energy will be radiated away in a similar manner to the one we have described in this study.

The expected lightcurve from a quasi-circular binary of NS that undergoes a prompt collapse will consist also with a precursor signal. In order to produce the lightcurve we use an analytic formula for the expected precursor signal in the case where only one NS is magnetised, this case is resembled in our study with the **Anti-Al<sub>2</sub>** model. The luminosity of such a binary is:

$$L_{\text{EM}} \simeq 3 \times 10^{41} b_{12}^2 (-t)^{-7/4} \text{ ergs}^{-1}. \quad (9)$$

where  $t$  the time to merger is measured in seconds and  $b_{12}$  as before ([Hansen & Lyutikov 2001](#); [Lyutikov 2011](#), [2018](#)). Equation (9) would overestimate the luminosity as the system approaches merger, diverging at the merger point. Thus, we use the results from ([Palenzuela et al. 2013a](#)) where they report the luminosity prior to merger, for a binary neutron star system where the magnetic dipoles are anti-aligned, scales like:  $L_{\text{EM}} \propto \Omega^{3/2}$ , where  $\Omega$  is the orbital frequency of the binary. This is smoothly joint with the previous analytic expression for the last one hundred milliseconds before merger. In fig. 9 we combine these formulas with our numerical results

to represent the expected EM luminosity for the case of quasi-circular binary that undergoes a prompt collapse to a BH in the first 0.5ms.

The latest detection of GW from a BNS merger, GW190425, unveiled a binary with a total mass of  $3.4^{+0.3}_{-0.1} M_{\odot}$ , which is rather unusual with regard to the binaries observed in our galaxy, and is consistent with a distance of  $159^{+69}_{-71}$  Mpc (The LIGO Scientific Collaboration et al. 2020). The current status about a binary of this total mass, expects a prompt collapse to a BH (Bauswein et al. 2013; Hotokezaka et al. 2011; Köppel et al. 2019; Agathos et al. 2019). We will use the toy model presented in this study in order to set limits on the flux expected from a BNS merging at the distance of GW190425. We assume that the magnetic loops radiated in our simulations dissipate magnetic energy through magnetic reconnection and a fraction of this is emitted as high-energy photons at the energy range of satellites that search for triggers of burst -like events, such as *Swift* (BAT), *Fermi* (GBM) and *INTEGRAL*. The estimated flux is:

$$F_X = f \frac{L}{4\pi d_L^2}. \quad (10)$$

where  $L$  is the luminosity coming from the simulation,  $d_L$  is the luminosity distance and  $f$  the fraction of the luminosity that dissipates in high-energy photons, which we assume to be  $f = 10\%$ , since similar values are found from kinetic simulations for dissipation through reconnection in pulsar magnetospheres (Philippov & Spitkovsky 2014; Cerutti et al. 2015; Brambilla et al. 2018; Crinquand et al. 2019).

The expected flux is shown in fig. 10, for a detection of a BNS that supposedly promptly collapsed to a BH, at a distance of  $159^{+69}_{-71}$  Mpc, where the upper and lower limits on the distance correspond to the upper and lower flux limits shaded in blue, also shown are the limits of the high-energy detectors from *Swift* (BAT) Barthelmy et al. (2005), *Fermi* (GBM) Meegan et al. (2009) and *INTEGRAL* (IBAS) Mereghetti et al. (2003). From the analysis provided by our modeling it is evident that a detection would not be possible, since the distance to the source is placing the expected flux exactly below the limits of the detectors. As a last remark, we should point out that in terms of radio, such a BNS is expected to have a radio luminosity with an efficiency of  $10^{-3} - 10^{-7}$  (Szary et al. 2014), since all observed pulsars have a similar radio efficiency when comparing the expected radiation from the magnetosphere with the observed one, and thus is extremely far to discuss any possibility for detection.

## 6. CONCLUSIONS

In the dawn of the multi-messenger era, where GW and EM radiation can be observed simultaneously from the merger of binary NS systems, any attempt of clarifying

such physical picture is invaluable. In this respect, the understanding of the dissipation of the magnetic energy of the two NS, when the system quickly undergoes a collapse to a BH, with no disk (or a minor disk) surrounding it, is of great importance. In this study we have followed a more idealized case of the head on collision of two NSs, in order to study the radiated EM energy produced during such collisions.

We have presented a comprehensive study of the head on collision of two magnetised NS. We have performed simulations with different initial magnetic field configurations and strengths. We have further deduced the efficiency of dissipating the available energy stored in both magnetospheres. We have shown that in the case of two anti-aligned magnetic dipoles the EM luminosity has an excess of two orders of magnitude, compared with the respective one coming from the merger of two stars with aligned dipoles, this result has been reported in studies of precursor signals (Palenzuela et al. 2013a). Our results were closely compared with the respective collapse of a magnetised NS. The EM luminosity is dictated by the collapse timescale and the magnetic energy stored in the magnetosphere, and not by the head-on collision assumption, this is the reason why we can use this study as a toy model and a conservative estimate for the EM output of a BNS prompt collapse to a BH, since the collapse timescale in this case is close to  $\sim 1$  ms.

Lastly, we discussed the resemblance of such EM signals of millisecond duration with the phenomenology of FRBs. We further discussed the possibility that such signals may originate from BNS mergers that undergo prompt collapse, and provided the expected high-energy flux limits, according to our analysis with respect to the GW detection GW190425, concluding that it would not be possible to trigger any of the satellite detectors considered.

## ACKNOWLEDGEMENTS

The author is thankful to L. Rezzolla and E. Most for useful discussions. AN is partially supported by an Alexander von Humboldt Fellowship. Partial support comes from “NewCompStar”, COST Action MP1304. The simulations were performed on SuperMUC at LRZ-Munich, on LOEWE at CSC-Frankfurt and on Hazelhen at HLRS in Stuttgart.

## REFERENCES

- Abbott B. P., et al., 2017, *Astrophys. J. Lett.*, 848, L13
- Agathos M., Zappa F., Bernuzzi S., Perego A., Breschi M., Radice D., 2019, arXiv e-prints, p. [arXiv:1908.05442](https://arxiv.org/abs/1908.05442)
- Alic D., Bona-Casas C., Bona C., Rezzolla L., Palenzuela C., 2012, *Phys. Rev. D*, 85, 064040
- Alic D., Kastaun W., Rezzolla L., 2013, *Phys. Rev. D*, 88, 064049
- Baiotti L., Rezzolla L., 2017, *Rept. Prog. Phys.*, 80, 096901

- Baiotti L., Giacomazzo B., Rezzolla L., 2008, *Phys. Rev. D*, **78**, 084033
- Barthelmy S. D., et al., 2005, *Space Science Reviews*, **120**, 143
- Baumgarte T. W., Shapiro S. L., 2002
- Bauswein A., Baumgarte T. W., Janka H.-T., 2013, *Phys. Rev. Lett.*, **111**, 131101
- Bovard L., Martin D., Guercilena F., Arcones A., Rezzolla L., Korobkin O., 2017, *Phys. Rev. D*, **96**, 124005
- Brambilla G., Kalapotharakos C., Timokhin A. N., Harding A. K., Kazanas D., 2018, *Astrophys. J.*, **858**, 81
- Bucciantini N., Del Zanna L., 2013, *Mon. Not. R. Astron. Soc.*, **428**, 71
- Cerutti B., Philippov A., Parfrey K., Spitkovsky A., 2015, *Mon. Not. R. Astron. Soc.*, **448**, 606
- Ciolfi R., Kastaun W., Giacomazzo B., Endrizzi A., Siegel D. M., Perna R., 2017, *Phys. Rev. D*, **95**, 063016
- Colella P., Sekora M. D., 2008, *Journal of Computational Physics*, **227**, 7069
- Crinquant B., Cerutti B., Dubus G., 2019, *Astron. Astrophys.*, **622**, A161
- Dietrich T., Ujevic M., 2017, *Classical and Quantum Gravity*, **34**, 105014
- Dietrich T., Ujevic M., Tichy W., Bernuzzi S., Brüggmann B., 2017a, *Phys. Rev. D*, **95**, 024029
- Dietrich T., Bernuzzi S., Tichy W., 2017b, *Phys. Rev. D*, **96**, 121501
- Dionysopoulou K., Alic D., Palenzuela C., Rezzolla L., Giacomazzo B., 2013, *Phys. Rev. D*, **88**, 044020
- Dionysopoulou K., Alic D., Rezzolla L., 2015, *Phys. Rev. D*, **92**, 084064
- East W. E., Pretorius F., 2013, *Phys. Rev. Lett.*, **110**, 101101
- Falcke H., Rezzolla L., 2014, *Astron. Astrophys.*, **562**, A137
- Fernández R., Tchekhovskoy A., Quataert E., Foucart F., Kasen D., 2018, *Mon. Not. R. Astron. Soc.*,
- Foucart F., O'Connor E., Roberts L., Kidder L. E., Pfeiffer H. P., Scheel M. A., 2016, *Phys. Rev. D*, **94**, 123016
- Fujibayashi S., Sekiguchi Y., Kiuchi K., Shibata M., 2017, *Astrophys. J.*, **846**, 114
- Fujibayashi S., Kiuchi K., Nishimura N., Sekiguchi Y., Shibata M., 2018, *Astrophys. J.*, **860**, 64
- Gundlach C., Martin-Garcia J. M., Calabrese G., Hinder I., 2005, *Class. Quantum Grav.*, **22**, 3767
- Hanauske M., Takami K., Bovard L., Rezzolla L., Font J. A., Galeazzi F., Stöcker H., 2017, *Phys. Rev. D*, **96**, 043004
- Hansen B. M. S., Lyutikov M., 2001, *Mon. Not. R. Astron. Soc.*, **322**, 695
- Harutyunyan A., Nathanail A., Rezzolla L., Sedrakian A., 2018, *European Physical Journal A*, **54**, 191
- Hotokezaka K., Piran T., 2015, *Mon. Not. R. Astron. Soc.*, **450**, 1430
- Hotokezaka K., Kyutoku K., Okawa H., Shibata M., Kiuchi K., 2011, *Phys. Rev. D*, **83**, 124008
- Hotokezaka K., Piran T., Paul M., 2017, in Kubono S., Kajino T., Nishimura S., Isobe T., Nagataki S., Shima T., Takeda Y., eds, 14th International Symposium on Nuclei in the Cosmos (NIC2016). p. 010608 ([arXiv:1510.00711](https://arxiv.org/abs/1510.00711)), doi:10.7566/JPSCP.14.010608
- Kastaun W., Galeazzi F., Alic D., Rezzolla L., Font J. A., 2013, *Phys. Rev. D*, **88**, 021501
- Kastaun W., Ciolfi R., Endrizzi A., Giacomazzo B., 2016a, preprint, ([arXiv:1612.03671](https://arxiv.org/abs/1612.03671))
- Kastaun W., Ciolfi R., Giacomazzo B., 2016b, *Phys. Rev. D*, **94**, 044060
- Kellerman T., Rezzolla L., Radice D., 2010, *Class. Quantum Grav.*, **27**, 235016
- Kiuchi K., Kyutoku K., Sekiguchi Y., Shibata M., Wada T., 2014, *Phys. Rev. D*, **90**, 041502
- Kiuchi K., Sekiguchi Y., Kyutoku K., Shibata M., Taniguchi K., Wada T., 2015, *Phys. Rev. D*, **92**, 064034
- Köppel S., Bovard L., Rezzolla L., 2019, *Astrophys. J. Lett.*, **872**, L16
- Lai D., 2012, *Astrophys. J. Lett.*, **757**, L3
- Lasky P. D., Haskell B., Ravi V., Howell E. J., Coward D. M., 2014, *Phys. Rev. D*, **89**, 047302
- Lehner L., Liebling S. L., Palenzuela C., Caballero O. L., O'Connor E., Anderson M., Neilsen D., 2016, *Classical and Quantum Gravity*, **33**, 184002
- Liu Y. T., Shapiro S. L., Etienne Z. B., Taniguchi K., 2008, *Phys. Rev. D*, **78**, 024012
- Löffler F., et al., 2012, *Class. Quantum Grav.*, **29**, 115001
- Lyutikov M., 2011, *Phys. Rev. D*, **83**, 124035
- Lyutikov M., 2018, preprint, ([arXiv:1809.10478](https://arxiv.org/abs/1809.10478))
- Margalit B., Metzger B. D., 2019, *Astrophys. J. Lett.*, **880**, L15
- Meegan C., et al., 2009, *Astrophys. J.*, **702**, 791
- Mereghetti S., Götz D., Borkowski J., Walter R., Pedersen H., 2003, *Astron. Astrophys.*, **411**, L291
- Metzger B. D., Zivancev C., 2016, *Mon. Not. R. Astron. Soc.*, **461**, 4435
- Most E. R., Nathanail A., Rezzolla L., 2018, *Astrophys. J.*, **864**, 117
- Nathanail A., 2018, *Astrophys. J.*, **864**, 4
- Nathanail A., Most E. R., Rezzolla L., 2017, *Mon. Not. R. Astron. Soc.*, **469**, L31
- Nathanail A., Porth O., Rezzolla L., 2019, *Astrophys. J. Lett.*, **870**, L20
- Palenzuela C., 2013, *Mon. Not. R. Astron. Soc.*, **431**, 1853
- Palenzuela C., Lehner L., Liebling S. L., Ponce M., Anderson M., Neilsen D., Motl P., 2013a, *Phys. Rev. D*, **88**, 043011
- Palenzuela C., Lehner L., Ponce M., Liebling S. L., Anderson M., Neilsen D., Motl P., 2013b, *Phys. Rev. Lett.*, **111**, 061105
- Palenzuela C., Liebling S. L., Neilsen D., Lehner L., Caballero O. L., O'Connor E., Anderson M., 2015, *Phys. Rev. D*, **92**, 044045
- Papenfort L. J., Gold R., Rezzolla L., 2018, *Phys. Rev. D*, **98**, 104028
- Pareschi L., Russo G., 2005, *Journal of Scientific Computing*, **25**, 129
- Paschalidis V., Ruiz M., 2018, preprint, ([arXiv:1808.04822](https://arxiv.org/abs/1808.04822))
- Paschalidis V., Etienne Z., Liu Y. T., Shapiro S. L., 2011, *Phys. Rev. D*, **83**, 064002
- Philippov A. A., Spitkovsky A., 2014, *Astrophys. J.*, **785**, L33
- Piro A. L., 2012, *Astrophys. J.*, **755**, 80
- Piro A. L., Giacomazzo B., Perna R., 2017, *Astrophys. J. Lett.*, **844**, L19
- Ponce M., Palenzuela C., Lehner L., Liebling S. L., 2014, *Phys. Rev. D*, **90**, 044007
- Pozanenko A. S., Minaev P. Y., Grebenev S. A., Chelovekov I. V., 2019, arXiv e-prints, p. [arXiv:1912.13112](https://arxiv.org/abs/1912.13112)
- Radice D., Galeazzi F., Lippuner J., Roberts L. F., Ott C. D., Rezzolla L., 2016, *Mon. Not. R. Astron. Soc.*, **460**, 3255
- Radice D., Perego A., Hotokezaka K., Fromm S. A., Bernuzzi S., Roberts L. F., 2018, *Astrophys. J.*, **869**, 130
- Rane A., Lorimer D., 2017, *Journal of Astrophysics and Astronomy*, **38**, 55
- Reisswig C., Haas R., Ott C. D., Abdikamalov E., Mösta P., Pollney D., Schnetter E., 2013, *Phys. Rev. D*, **87**, 064023
- Rezzolla L., Takami K., 2013, *Class. Quantum Grav.*, **30**, 012001
- Rezzolla L., Giacomazzo B., Baiotti L., Granot J., Kouveliotou C., Aloy M. A., 2011, *Astrophys. J. Letters*, **732**, L6
- Ruderman M. A., Sutherland P. G., 1975, *Astrophys. J.*, **196**, 51
- Ruiz M., Shapiro S. L., 2017, *Phys. Rev. D*, **96**, 084063
- Ruiz M., Lang R. N., Paschalidis V., Shapiro S. L., 2016, *Astrophys. J. Lett.*, **824**, L6



- Ruiz M., Shapiro S. L., Tsokaros A., 2018, [Phys. Rev. D](#), **97**, 021501
- Schnetter E., Hawley S. H., Hawke I., 2004, [Class. Quantum Grav.](#), **21**, 1465
- Sekiguchi Y., Kiuchi K., Kyutoku K., Shibata M., 2015, [Phys. Rev. D](#), **91**, 064059
- Sekiguchi Y., Kiuchi K., Kyutoku K., Shibata M., Taniguchi K., 2016, [Phys. Rev. D](#), **93**, 124046
- Shibata M., Taniguchi K., 2006, [Phys. Rev. D](#), **73**, 064027
- Shibata M., Suwa Y., Kiuchi K., Ioka K., 2011, [Astrophys. J.](#), **734**, L36
- Siegel D. M., Metzger B. D., 2018, [Astrophys. J.](#), **858**, 52
- Sturrock P. A., 1971, [Astrophys. J.](#), **164**, 529
- Szary A., Zhang B., Melikidze G. I., Gil J., Xu R.-X., 2014, [Astrophys. J.](#), **784**, 59
- The LIGO Scientific Collaboration et al., 2020, arXiv e-prints, [p. arXiv:2001.01761](#)
- Wang J.-S., Yang Y.-P., Wu X.-F., Dai Z.-G., Wang F.-Y., 2016, [Astrophys. J. Lett.](#), **822**, L7
- Zhang B., 2016, [Astrophys. J. Lett.](#), **827**, L31